LA-UR- 92-371

LA-UR--92-371

DE92 008444

TITLE: MODELING OF TRANSFORMATION TOUGHENING IN BRITTLE MATERIALS

AUTHOR(S): R. LeSar
A. D. Rollett
D. J. Srolovitz*

SUBMITTED TO: High Temperature Structural Silicides Workshop, Gaithersberg, MD November 4-6, 1991

*Department of Materials Science and Engineering, University of Michigan, Ann Arbor, MI 48109

Los Alamos National Laboratory
Los Alamos, New Mexico 87545

Modeling of Transformation Toughening in Brittle Materials

R. LeSar and A. D. Rollett
Los Alamos National Laboratory
Los Alamos, NM 87545

D. J. Srolovitz
University of Michigan
Ann Arbor, MI 48109

Abstract

Results from modeling of transformation toughening in brittle materials using a discrete micromechanical model are presented. The material is represented as a two-dimensional triangular array of nodes connected by elastic springs. Microstructural effects are included by varying the spring parameters for the bulk, grain boundaries, and transforming particles. Using the width of the damage zone and the effective compliance (after the initial creation of the damage zone) as measures of fracture toughness, we find that there is a strong dependence of toughness on the amount, size, and shape of the transforming particles, with the maximum toughness achieved with the higher amounts of the larger particles.

§I. Introduction

A number of approaches have been taken to improve the fracture toughness of brittle materials. One such approach, called transformation toughening, involves including particles of metastable tetragonal zirconia (ZrO_2) that undergo a martensitic transformation to the larger-volume (+4%) monoclinic structure in the stress field near the vicinity of a crack tip [1]. The zirconia particles are stabilized in the tetragonal structure by alloying and by the constraints of the ceramic matrix. High stresses can trigger the irreversible transition to the stable monoclinic structure in a region around the crack tip, referred to as the transformation zone. This approach has been used to improve the fracture toughness of alumina-zirconia composites [2]. Recent work by Petrovic and coworkers [3-5] demonstrated that dispersed particles of stabilized ZrO_2 also increases the fracture toughness of $MoSi_2$-based materials.

There have been many theoretical studies of transformation toughening that have tried to correlate the increase in toughness to the size and shape of the transformation zone around the crack tip [6]. Generally, these studies have modeled the transformation zone as a linear-elastic continuum, and have considered the case of dilatational transformations triggered by a critical mean stress. Recently, Stump [7] has extended the continuum-mechanics approach to include the effects of a discrete array of particles. This was done by embedding a random distribution of small, discrete, circular inclusions in an elastic matrix surrounding the tip of a semi-infinite crack. These inclusions could undergo a transformation when the stress on them was greater than a set amount. Prior to transformation, the spots and matrix were homogeneous, linear elastic media described by isotropic constants E and ν. Stump considered not only the usual case of purely dilatational transformations triggered by a mean-stress criterion but also the general case with shear

transformation stresses and strains. He related the size and shape of the transformation zone as a function of the transformation criteria to the fracture toughness.

One drawback to the continuum mechanics calculations is that it is difficult to include the effects of microstructure on the fracture properties of the material. Additionally, the continuum mechanics results were restricted to the case of the transformation zone around a stationary crack. Experiments [5] show that there is considerable microcracking around the transformed particles. To examine the role of microstructure and microcracking, we have taken another approach, namely a ball-and-spring model [8,9]. In the next section we shall outline the approach as applied to transformation toughening and describe the role of microstructure on the damage zone in a strained material.

§II. Discrete Micromechanical Model

Extension of the modeling to include the effects of microstructure and microcracking requires a different approach than that used in the partially-discrete micromechanical model developed by Stump [7]. We use a "ball-and-spring" approach, where we treat the system as a two-dimensional triangular lattice of nodes, each of which is connected to its six nearest neighbors by elastic springs. The energy of this system is given by

$$E = \frac{1}{2} \sum_{i=1}^{N} \sum_{j=1}^{6} k_{ij} (r_{ij} - r^{o}_{ij})^{2}$$

where k_{ij} is the force constant and r_{ij}^{o} is the equilibrium length of the spring connecting node i to node j. Fracture occurs when the spring length, r_{ij}, exceeds the

breaking strain, r_{ij}^b. The unstressed topology of the model is shown in Figure 1. We note that the elastic properties of this system are those of an isotropic solid. While the model can be improved by including 3-body (angular) interactions [9], for the present study we restrict the model to two-body interactions.

The microstructure is generated with a Potts model, which has been shown to yield realistic grain-size distributions [10]. The Potts model is similar to an Ising model, except that, instead of having only two possible spin values, many values are allowed. Areas with different spin values correspond to different grains. A typical section of the system is shown in Figure 2. The line marking the region between grains is a grain boundary. S represents a second-phase particle. The key to the utility of the model is that springs can be assigned different parameters depending on whether they connect nodes within the same grain, nodes in different grains, or nodes connected to second-phase particles. Thus, we can model competing fracture mechanisms.

We assume that all bulk grains are alike and that there is no orientational dependence in the grain-boundary properties. Thus, all bulk springs (within the grains, e.g., the 1-1 interaction in Figure 2) are defined by the three spring parameters k_B, r_B^o, and r_B^b. The properties of springs crossing grain boundaries (e.g., 1-2 in Figure 2) are given by k_{gb}, r_{gb}^o, and r_{gb}^b. Similarly, springs connected to second-phase particles (e.g., S-1 in Figure 2) have properties k_S, r_S^o, and r_S^b. Transformation of a second-phase particle is modeled by irreversibly increasing the equilibrium spring length r_S^o to $r_S^{o,T}$ when the mean stress on the second-phase particle exceeds a prescribed critical stress, σ_c. For all the calculations described here, $k_B = k_{gb} = k_S = 1 = r_B^o = r_{gb}^o = r_S^o$. Based on a typical experimental value for ZrO_2, we assume that there is a 1% increase in the length of the springs connected to second phase particles upon transformation, i.e., $r_S^{o,T} = 1.01$. The breaking strain for the bulk bonds is $r_B^b = 1.005$ and for the grain boundaries and second phase

particles $r_{gb}^{b} = r_{S}^{b} = 1.003$. We note that this choice of breaking strains ensures that there should be a mixture of trans- and intergranular fracture [8]. Finally, we assume a mean-stress criterion for transformations with a critical stress $\sigma_c = 1.001$. These parameters were obviously not chosen to match the exact properties of $MoSi_2$, but rather to incorporate in an approximate way the basic phenomena associated with transformation toughening.

The calculations proceed as follows. An initial distribution of grain boundaries and second-phase particles is assigned to the system, which is then strained in the x direction (Figure 1) by a finite amount. The energy of the system is minimized with respect to the positions of the nodes. If the mean stress on any second-phase particles is greater than σ_c, then we transform the particle with the largest stress and minimize the energy with respect to positions again. We iterate until no more particles transform. We then check to see if any spring has a length greater than its breaking strain. If so, we irreversibly break the spring with the largest ratio of r_{ij} to r_{ij}^{b} and minimize the energy again. We iterate until no more springs break. We then check to see if any particles transform, and so on. Once no more particles transform and no more springs break, the strain is increased and the procedure is repeated. We note that the iterative procedure used here is not unique; other schemes are being investigated.

In Figure 3a, we show the basic microstructure of the 100x100 lattice of nodes used in all simulations reported here. The black lines are grain boundaries generated by a Potts model and the gray wide line is an initial crack created by breaking some of the springs prior to starting the calculations. The system was then strained in small discrete steps until fracture. Since the breaking strain of the springs is 0.003 for the weakest springs, we chose a strain step of 0.0001, which should provide sufficient resolution. In Figure 3b, we show the results for total strain of 0.003. Once again, the broad gray line is the fracture path. We note that

since periodic boundaries are used in the simulation, when the crack leaves the left hand side of the cell, it reappears on the right. In Figure 3c, we show the stress-strain curve for this case. We note that the material behaves completely elastically until a strain of 0.003 and then breaks completely. That the fracture was complete is seen by the flat stress as a function of strain, i.e., the material is being pulled apart with no resistance. Examining the fracture path in Figure 3b, we see that there is a mixture of inter- and transgranular fracture.

In Figure 4a, we show the initial condition for a case where we have included 10% (by number) second-phase particles (light gray) placed at random on the same microstructure as used in Figure 3. Applying a strain to the system results in markedly different behavior from the system with no second-phase particles. In Figure 4b, we show that the system is damaged at a strain of 0.0015, half that necessary for failure of the system with no transforming particles. We note that the crack is not continuous and fails to span the system, i.e., the system has not failed. A transformation zone develops in front of the initial crack tip and is accompanied by microcracking around the transforming particles, in agreement with experimental observations [5]. Straining the system further to a net strain of 0.003 yields Figure 4c. Note that the microcracks have seemingly coalesced into one, continuous crack. However, the stress-strain curve in Figure 4d does not show a flat response of stress versus strain as expected if the system had failed, thus indicating that the crack is not continuous across the system. Indeed, the system has not failed up to a total strain of 0.005. The damage was initiated at a strain half that of the material with no second-phase particles, an example, perhaps, of microshielding of the crack tip. If one were to use the critical stress as a measure of toughness, then it would imply that addition of second-phase particles actually impairs the properties of these materials. However, the fracture zone is broader than with no second-phase particles and the system can be strained to a significantly higher extent without

failure, so clearly a different definition of toughness is necessary. We shall return to this point below.

In Figure 5a, we show a system with 20% randomly placed second-phase particles at a strain of 0.0015. The most obvious difference between this case and that with 10% transforming particles (Figure 4b) is that the 20% system has a much broader transformation/damage zone. Once again, the system has clearly not failed at this stress. In Figure 5b, we show the same system at a strain of 0.003. The damage zone has broadened, but otherwise the system behaves very similarly to that with 10% particles. The stress-strain curve in Figure 5c indicates that the system has not failed at a strain of 0.005.

We show results with 30% randomly-placed second-phase particles at a strain of 0.0012 in Figure 6a. Note that a transformation zone (with microcracking) has developed in front of the crack tip. Comparison of the shape of the transformation zone with that found with the partially-discretized continuum mechanics [7] shows clear differences, largely associated with microcracking around the transforming particles, which is not included in the continuum mechanics calculations. In Figure 6b we show the 30% system with a strain of 0.0015 and in Figure 6c with a strain of 0.003. We note again that the overall behavior is very similar with 10%, 20%, and 30% second-phase particles, with the primary differences being the width of the transformation zone and the critical stress for onset of damage. One feature of the present model that may seem surprising is the negative stress (i.e., positive pressure) seen in the stress-strain curve for the case with 30% second-phase particles. The stress plotted in these figures is the total stress (xx component) of the system. When the particles transform, they occupy a larger volume, thus causing a local increase in pressure. In a real material, where the total transformation zone is a small part of the total volume, this would not be observable. However, the transformation zone is a large part of the small systems used in our model. Thus, the

total stress is dominated by what occurs in the transformation zone and the overall stress is negative.

To best compare the results with experiment requires a definition of the fracture toughness in our model. Examination of the fracture zones in Figure 4-6 clearly shows that a Griffiths analysis, which is designed for sharp cracks, is not appropriate. Thus, a different approach must be used. In Figure 7, we show the stress-strain curves for 0, 10, 20, 30, and 40% transforming particles (the calculation with 40% particles was stopped at a strain of 0.0035). As is clear, the critical strain for damage propagation for the systems with transforming particles is roughly half that of the material without additions. The critical stress is not, however, a good measure of the toughness of the material, since the systems with second-phase particles can be strained to much larger values without failure. Another measure of toughness might be the effective compliance (i.e., slope of the $\sigma-\varepsilon$ curve) of the material after creation of the damage zone, which should be a measure of the amount of elastic energy that can be stored in the material. From Figure 7, it is clear that there are some uncertainties in how this slope should be calculated. We used the slope of the line connecting the minimum and maximum of the stress-strain curve after the creation of the initial damage zone. That slope, which we define as the effective compliance after creation of the damage zone (k_{eff}), is plotted in Figure 8 as a function of amount of transforming particles in the system. We note that there is a slow rise in k_{eff} with small amounts of transforming particles, then a sharp rise, and a finally a leveling off.

Another measure of the amount of energy that can be stored in the system is the size of the damage zone, which we approximate as the width (Δ) of the damage zone at a strain of 0.003. This quantity, which is plotted in Figure 8, represents the area over which the damage is spread and that can absorb new damage. We note that the basic shape of the curves for k_{eff} and Δ are similar: a slow rise at small amounts

of second-phase particles, a steep rise, and then an apparent leveling off at large amounts of transforming particles. These quantities suggest that there is an amount of transforming particles that maximizes the toughness of the material. Such an effect has been noted in Al_2O_3/ZrO_2 composites, which show a maximum toughness at about 40 volume% ZrO_2 (see Figure 5 in Reference 5). One caveat that must be made about the present simulations, however, is that at 40 number% transforming particles, the fracture zone covers approximately half the entire system. Thus, the results must be verified with a larger system to examine possible system-size effects. Given Figure 8 as a measure of toughness, however, we see indications of a leveling off of toughness at high concentrations of transforming particles.

In the simulations just reported, we assumed a random distribution of small transforming particles, i.e., each particle was one node. An experimentally controllable parameter is, however, the size of the particles. In Figure 9, we show results for a case where we have created larger particles by designating a node and its 6 hexagonally-placed nearest neighbors as a transforming particle. Figure 9 corresponds to a total of 20% of all the nodes being transforming particles. We first note from the stress-strain curve that the critical stress for creation of the damage zone is 0.0019, somewhat higher than the 0.0015 needed for the case with small particles. Examination of the damage zone (Figure 9b) shows that it is considerably larger than the case with the same total concentration but with smaller particles (Figure 5). The width at a strain of 0.003 is approximately 0.45 of the cell size, considerably larger than the value (0.33) for the small particles at the same concentration. From the stress-strain curve, we find that the effective compliance is approximately 0.35, which is much larger than the value of 0.19 for the small particle case. Thus, it is clear that, by the measures used here, the material is tougher with the larger particles than with the smaller ones. We note that since the

large particles are made up of seven nodes, the entire particle need not transform at the same time. Examination of Figures 9b and 9c shows regions with some transformed and some untransformed second-phase material, in agreement with experiment [5].

We have also performed a number of calculations with a smaller system size (50x50) with qualitatively similar results. One interesting result concerned the effects of particle orientation on toughness. Using as the transforming particles (20% total concentration) sets of three nodes connected in straight lines (Figure 10), we found that the system with particles parallel to the strain direction (10b) to be considerably tougher (in Δ, k_{eff}, and critical stress) than a system with particles aligned perpendicular to the strain (10a) as well as a system with randomly-placed small particles. It may be possible to make samples with these sorts of particle distributions, so that these predictions can be verified. From Figure 10b, we see that the damage zone extends completely across the system, which is clearly unphysical. It is for this reason that it was necessary to consider the larger 100x100 systems used in the rest of the calculations reported here.

In summary, we have developed a model that incorporates the essential features of transformation toughening. We find that there is a strong dependence of the toughness on the amount, size, and shape of the transforming particles. We are currently developing better estimates of the parameters appropriate for application to $MoSi_2$-based composites. Given those, more explicit predictions can be made on the optimal particle distribution.

Acknowledgments

The authors (R.L. and A.D.R.) gratefully acknowledge the U. S. Department of Energy Advanced Industrial Concepts Materials Program for support of this work. Their work was performed under the auspices of the U. S. Department of Energy. D.J.S. acknowledges the support of the Air Force Office of Scientific Research's URI program (contract AFOSR-90-0112). We want to thank David M. Stump for helpful discussions. Calculations for the 50x50 system (Figure 10) were carried out by Valerie Dianne Pacheco and Hsin Tsao under the auspices of the Los Alamos Summer Science Student Program.

References

1. R. Stevens. "Zirconia and Zirconia Composites," Second Edition, (Magnesium Electron Ltd., Twickenham, U. K., 1986); A. G. Evans and R. M. Cannon, Acta. Metal., 34 (1986), 761; A. G. Evans and A. H. Heuer, J. Am. Ceram. Soc., 63 (1980), 241.

2. F. F. Lange, J. Mat Sci., 17 (1982), 247; J. Wang and R. Stevens, J. Mat. Sci., 24 (1989), 3421.

3. J. J. Petrovic and R. E. Honnell, J. Mat. Sci., 25 (1990), 4453.

4. J. J. Petrovic, R. E. Honnell, T. E. Mitchell, R. K. Wade, and K. J. McClellan, Proceedings, 15th Annual Conference on Composites and Advanced Ceramics, 13-16 January 1991, Cocoa Beach Florida.

5. J. J. Petrovic, A. K. Bhattacharya, R. E. Honnell, T. E. Mitchell, R. K. Wade, and K. J. McClellan, this volume.

6. R. M. McMeeking and A. G. Evans, J. Am. Ceram. Soc., 65 (1982), 242; B. Budiansky, J. W. Hutchinson, and J. C. Lambropoulos, Int. J. Solids and Structures, 19 (1983), 337; D. M. Stump and B. Budiansky, Int. J. Solids and Structures, 25 (1989), 635.

7. D. M. Stump, Phil. Mag. A, 64 (1991), 879.

8. W. H. Yang, D. J. Srolovitz, G. N. Hassold and M. P. Anderson, in "Simulation and Theory of Evolving Microstructures," Edited by M. P. Anderson and A. D. Rollett, (Minerals, Metals, and Materials Society, Warrendale, PA, 1990), 277.

9. D. J. Srolovitz, W. H. Wang, R. Najafabadi, H. Y. Wang, and R. LeSar, in "Atomic-Level Properties of Interface Materials," in press.

10. M. P. Anderson, D. J. Srolovitz, G. S. Grest, and P. S. Sahni, Acta Metal., 32 (1984), 783.

Figure Captions:

Figure 1: Topology of discrete micromechanical model. A two-dimensional triangular lattice of nodes connected by springs are used. The top and bottom are free surfaces and the sides have periodic boundary conditions. An initial crack of varying length is created at the bottom edge. The system is strained by pulling in the x direction.

Figure 2: Typical section of lattice of nodes. The lines drawn between areas with different numbers define grain boundaries. S represents a second-phase particle. Different parameters can be assigned to springs connecting nodes: within the bulk, across grain boundaries, or connected to second-phase particles. see text for details.

Figure 3: (a) Basic microstructure used in 100x100 simulations. The dark lines are grain boundaries and the heavy gray line is an initial crack. Note that we have tilted the figure by 30 degrees to better fit on the page (see Figure 1). (b) The system at a total strain of 0.003. Note that the crack has moved completely across the sample. Because of the periodic boundary conditions along the x-direction (Figure 1), the crack moved off the left hand side of the cell and back in on the right. (c) Stress-strain curve.

Figure 4: (a) Initial structure for a system with 10% randomly placed second-phase particles (in light gray) on the microstructure used in Figure 3. The solid lines are grain boundaries and the wide gray line is the initial crack. (b) System after a strain of 0.0015. The dark spots are transformed particles. (c) System after a strain of 0.003. (d) Stress-strain curve.

Figure 5: System with 20% randomly placed second-phase particles (in light gray) on the microstructure used in Figure 3. The solid lines are grain boundaries and the wide gray line is the initial crack. (a) System after a strain of 0.0015. The dark spots are transformed particles. (b) System after a strain of 0.003. (c) Stress-strain curve.

Figure 6: System with 30% randomly placed second-phase particles (in light gray) on the microstructure used in Figure 3. The solid lines are grain boundaries and the wide gray line is the initial crack. (a) System after a strain of 0.0012. The dark spots are transformed particles. (b) System after a total strain of 0.0015. (c) System after a strain of 0.003. (c) Stress-strain curve.

Figure 7: Stress-strain curves for the cases with 0, 10, 20, 30 and 40% transforming particles.

Figure 8: Approximate effective compliance k_{eff}, as defined in the text (solid line), and width of fracture zone Δ, as a fraction of cell size (dashed line), as a function of amount of second-phase particles.

Figure 9: System with 20% randomly placed second-phase particles (in light gray) on the 100x100 microstructure used in Figure 3. The particles were created as a combination of a central node and its six hexagonal nearest neighbors. The solid lines are grain boundaries and the wide gray lines are the cracks. (a) Initial conditions. (b) System after a strain of 0.0019. The dark spots are transformed particles. (c) System after a strain of 0.003. (d) Stress-strain curve.

Figure 10: System with 20% randomly placed second-phase particles (in light

gray) in a system of 50x50 nodes. The particles were created as a combination of three nodes, aligned either perpendicular (a) or parallel (b) to the direction of strain. The solid lines are grain boundaries and the wide gray lines are the cracks. Shown are results at a strain of 0.003.

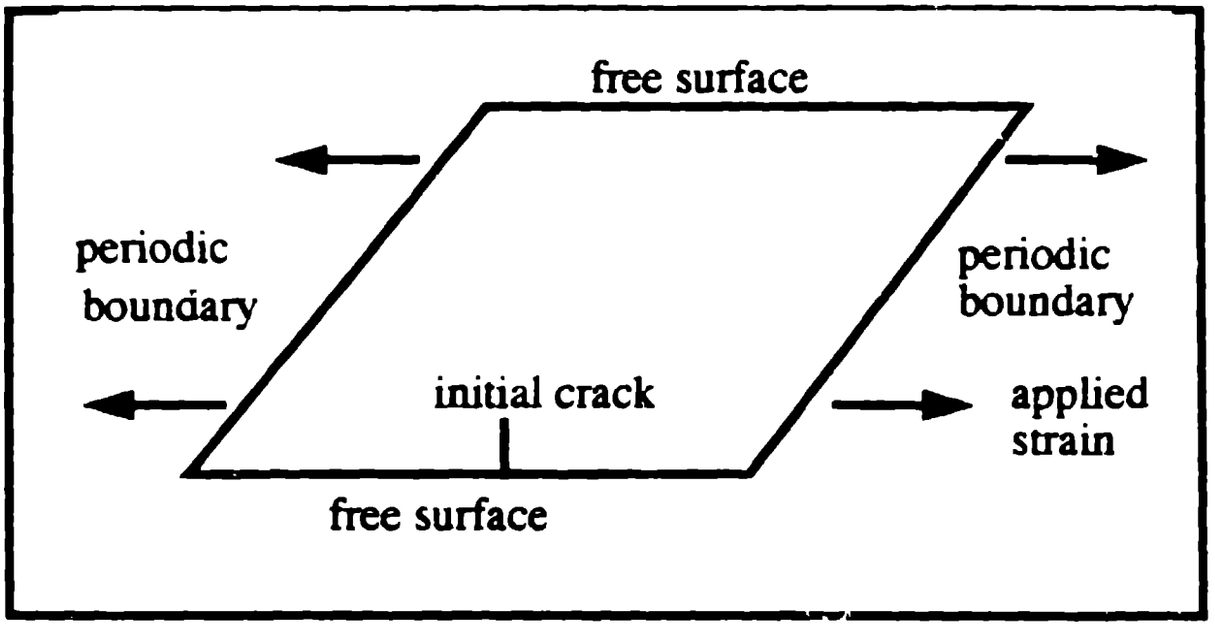
free surface
periodic
boundary
periodic
boundary
initial crack
applied
strain
free surface

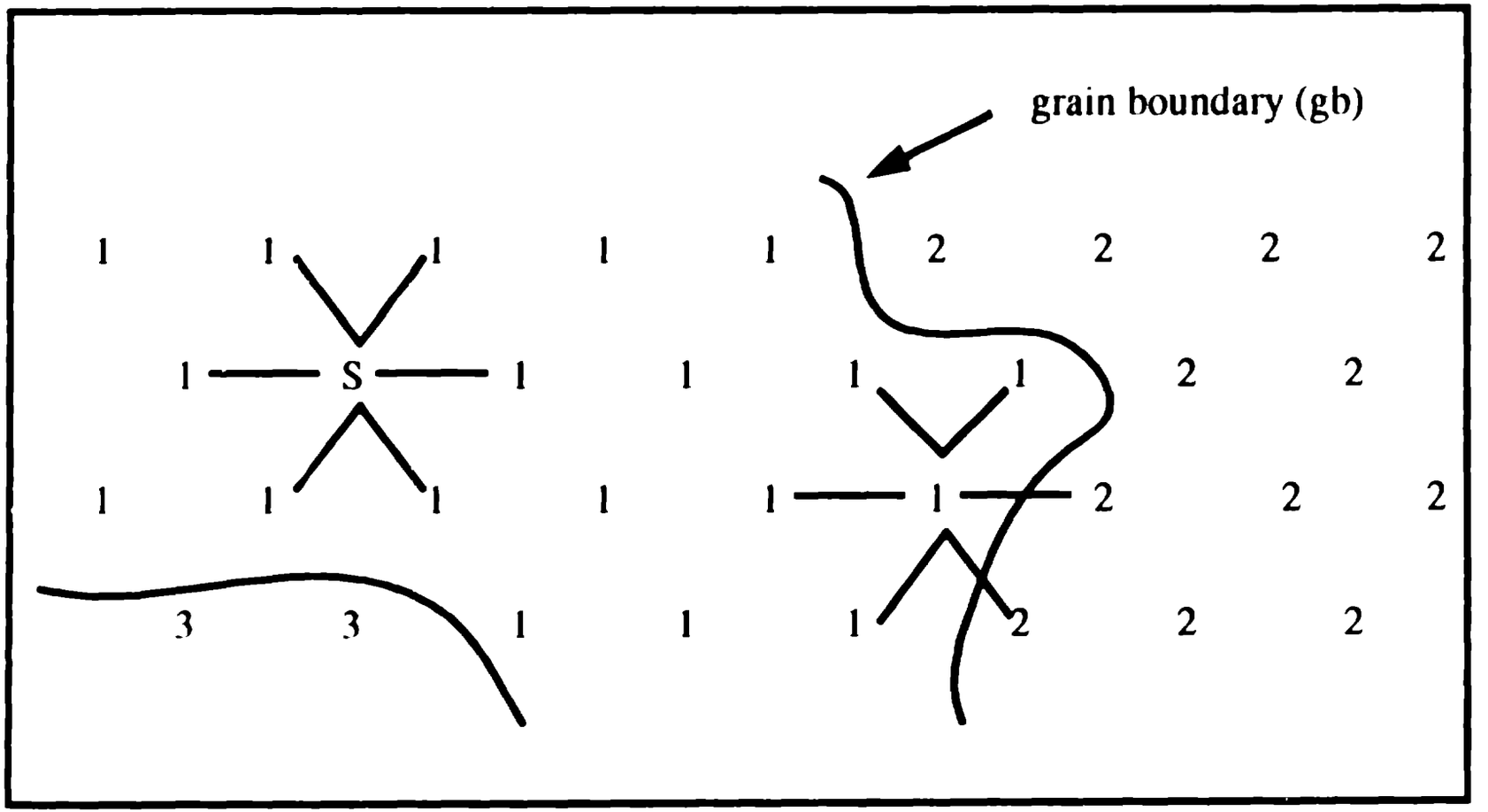
grain boundary (gb)
S

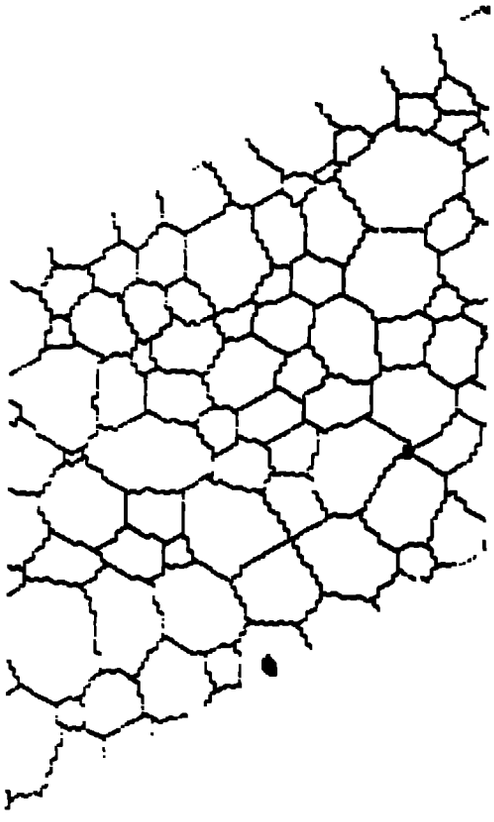

(a)

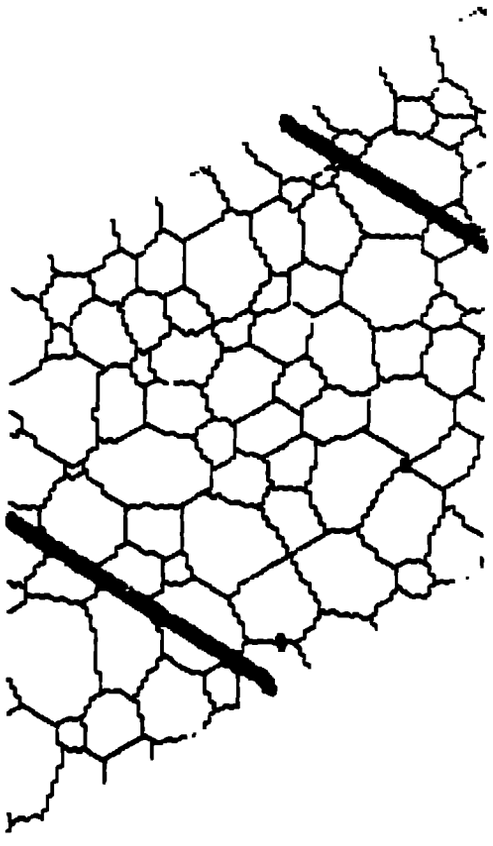

(b)

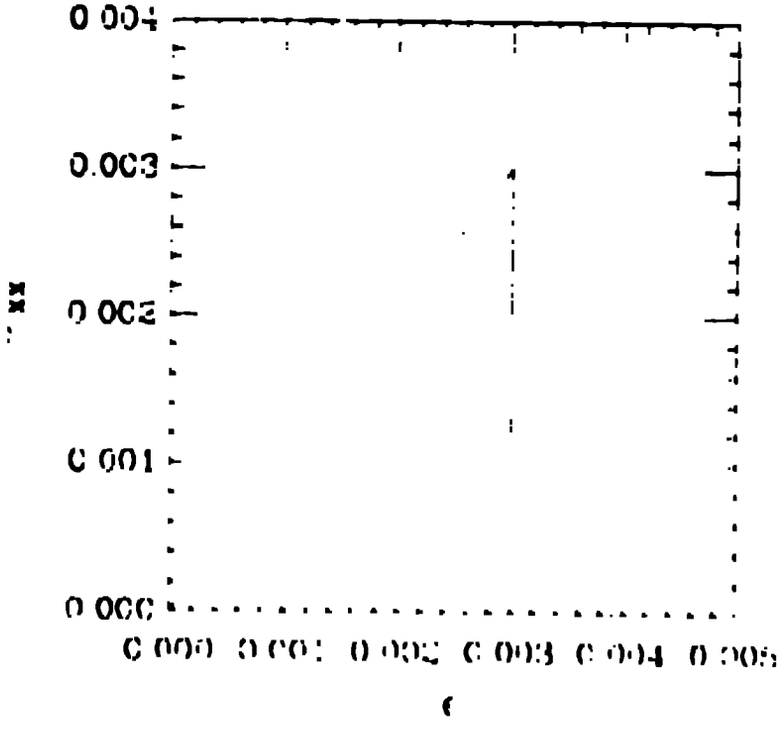

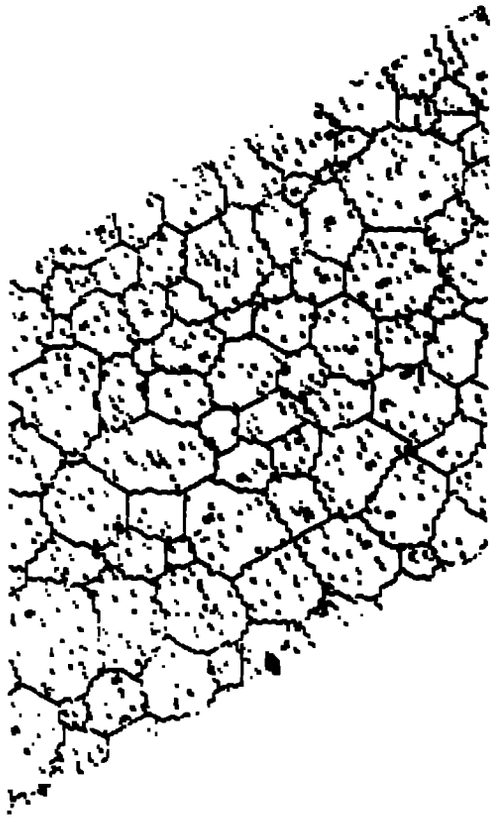

(a)

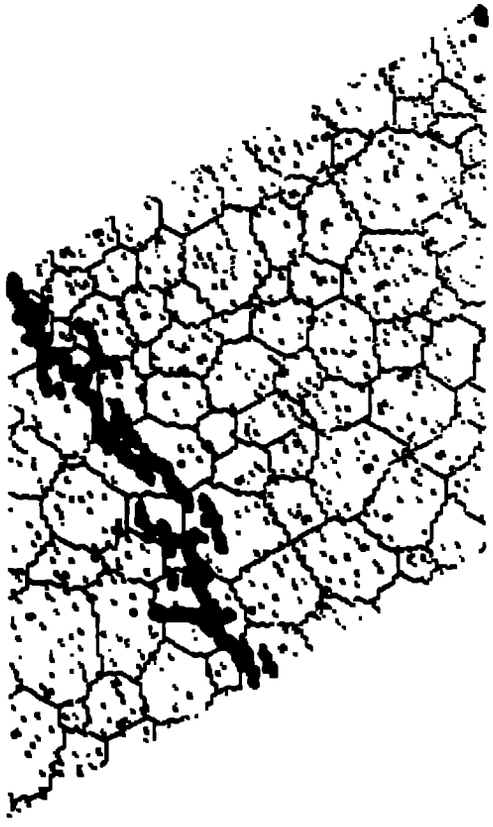

(b)

(c)

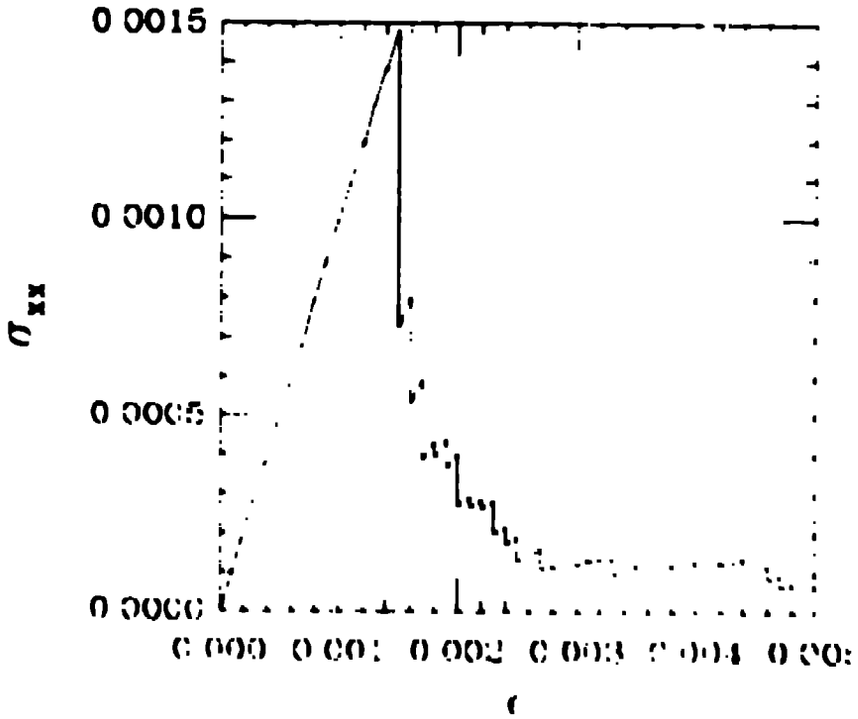
0 0015
0 0010
0 0005
0 0000
0 000
0 001
0 002
0 003
0 004
0 00
σ_{xx}
ϵ

(d)

(a)

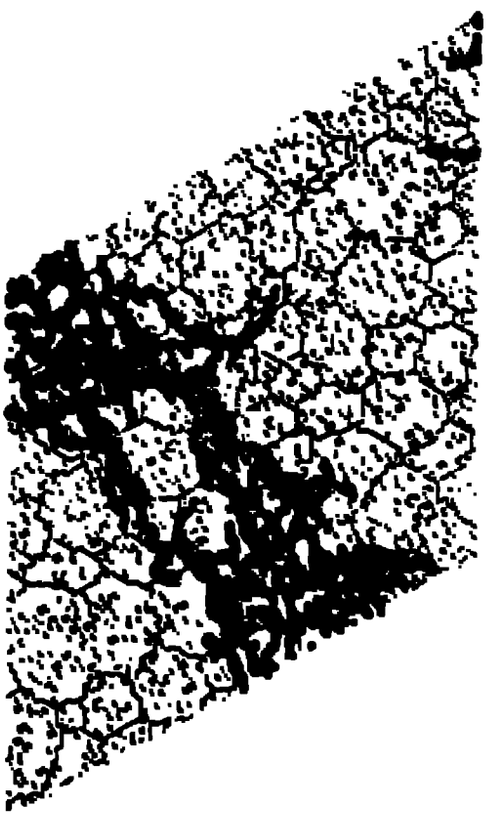

(b)

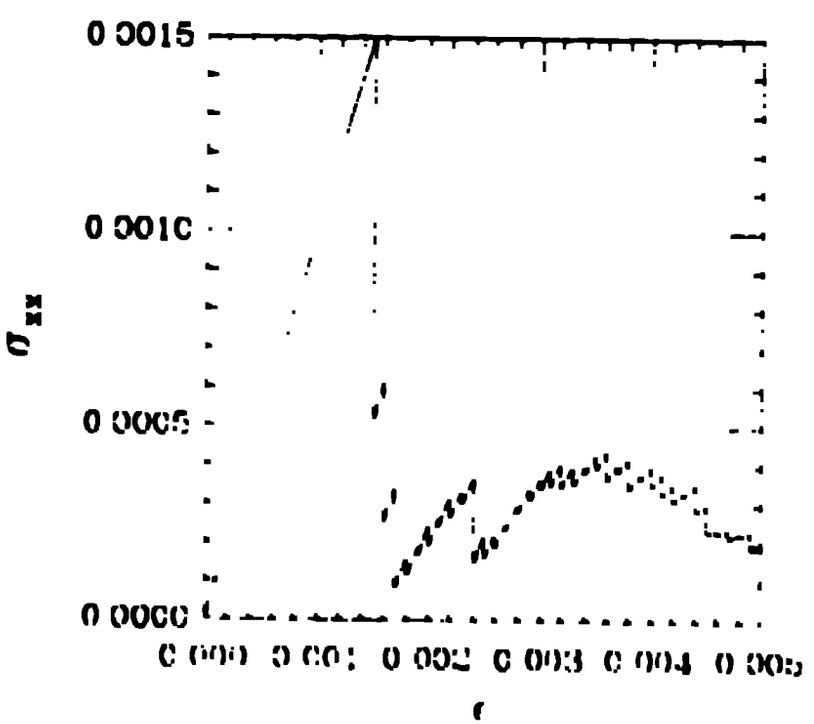
0 0015
0 0010
0 0005
0 0000
σ_{xx}
0 000 0 001 0 002 0 003 0 004 0 005
ϵ

(c)

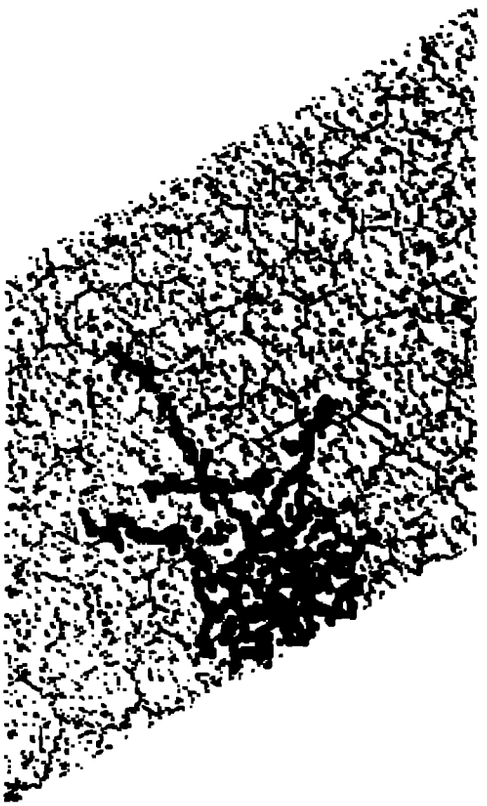

(a)

(b)

(c)

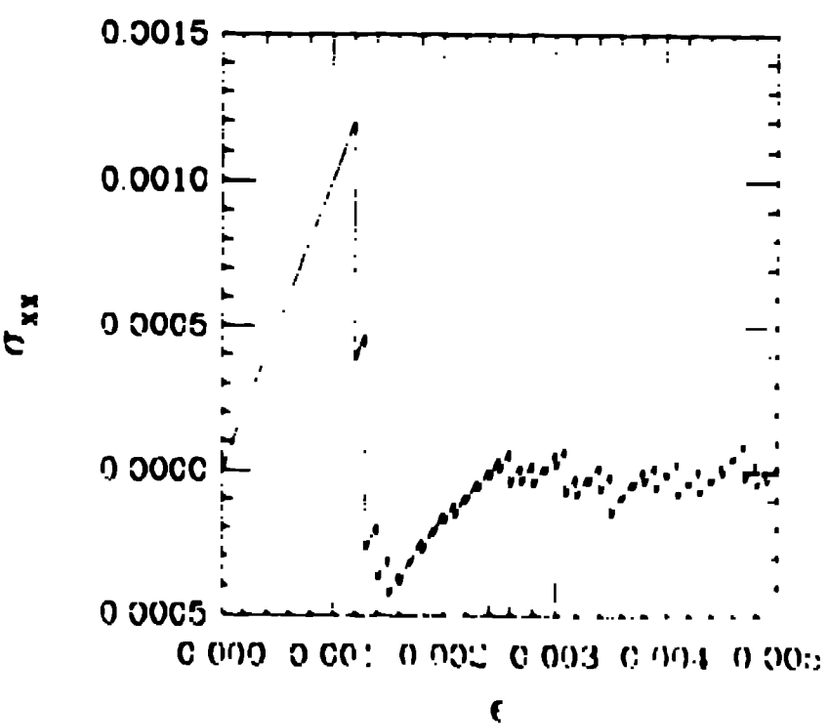

(d)

Figure 6

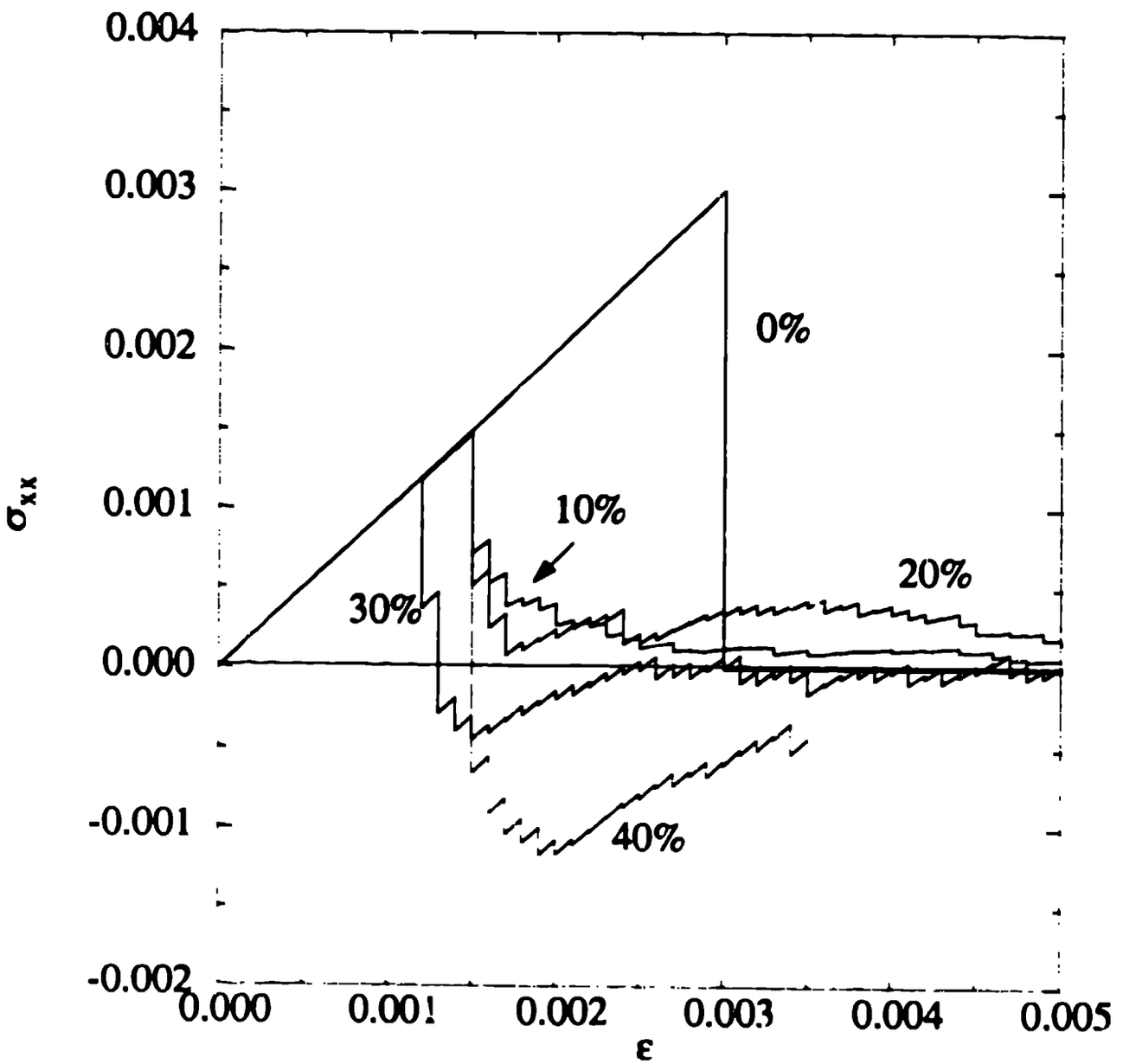
0.004
0.003
0.002
0.001
0.000
-0.001
-0.002
σ_{xx}
0.000
0.001
0.002
0.003
0.004
0.005
ε
0%
10%
20%
30%
40%

Figure 7

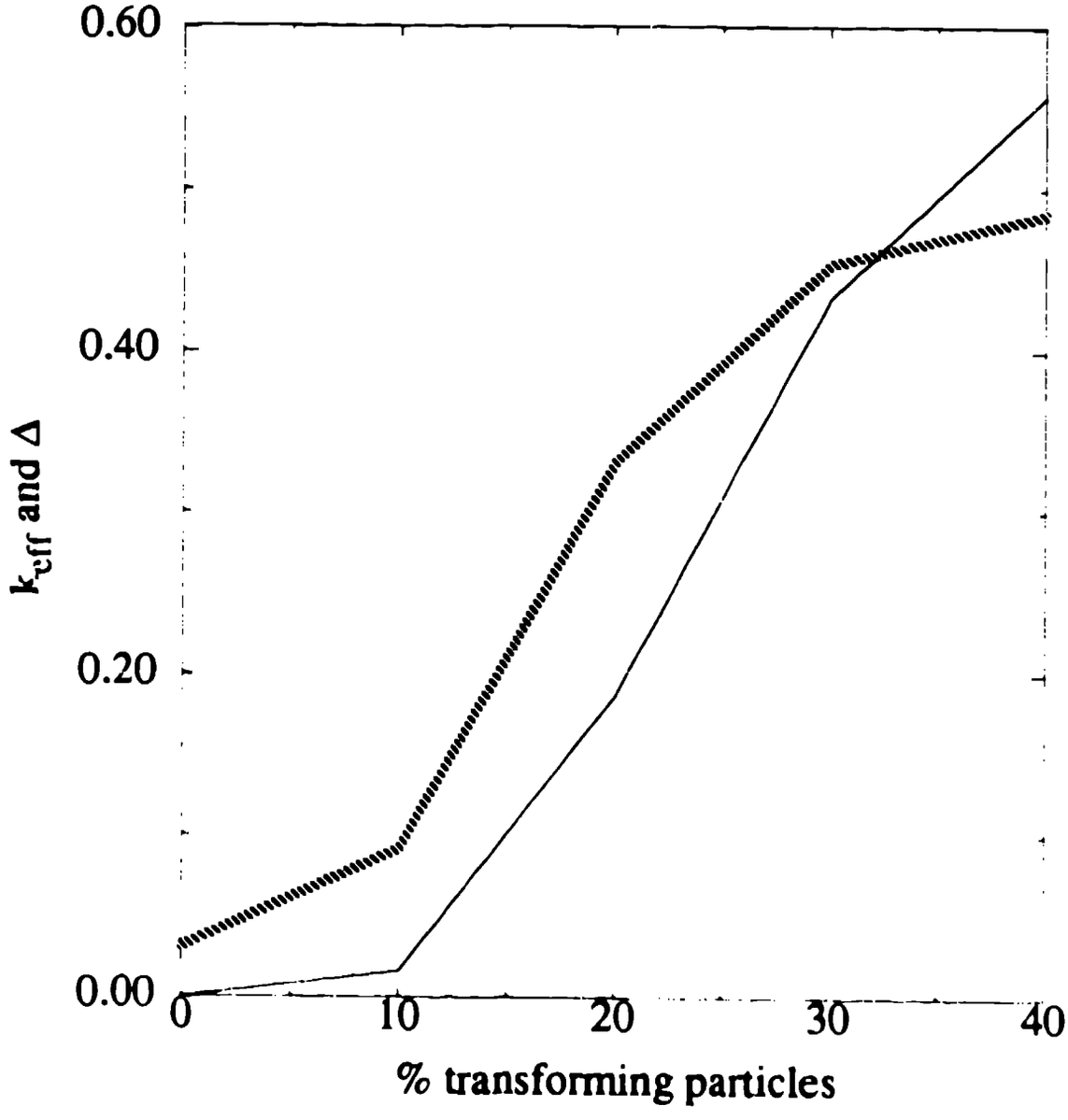
0.60
0.40
0.20
0.00
k_{eff} and Δ
0
10
20
30
40
% transforming particles

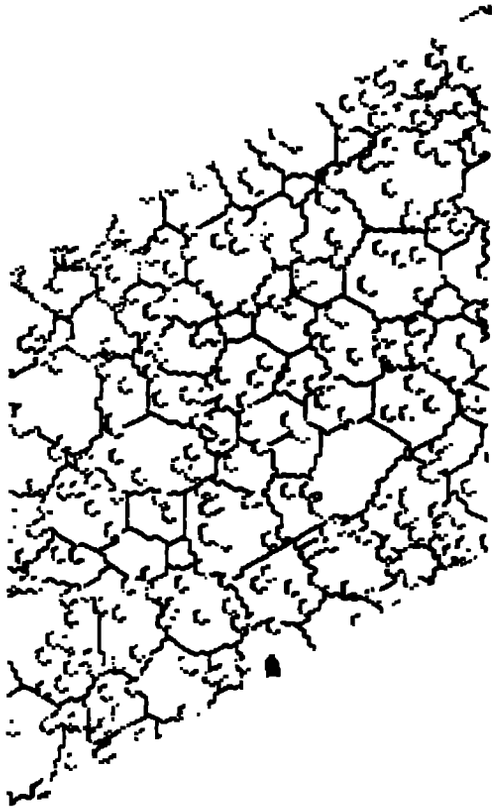

(a)

(b)

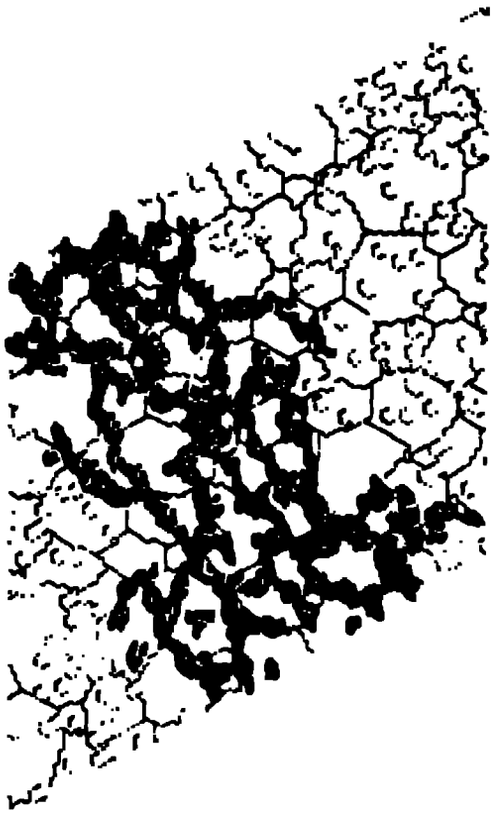

(c)

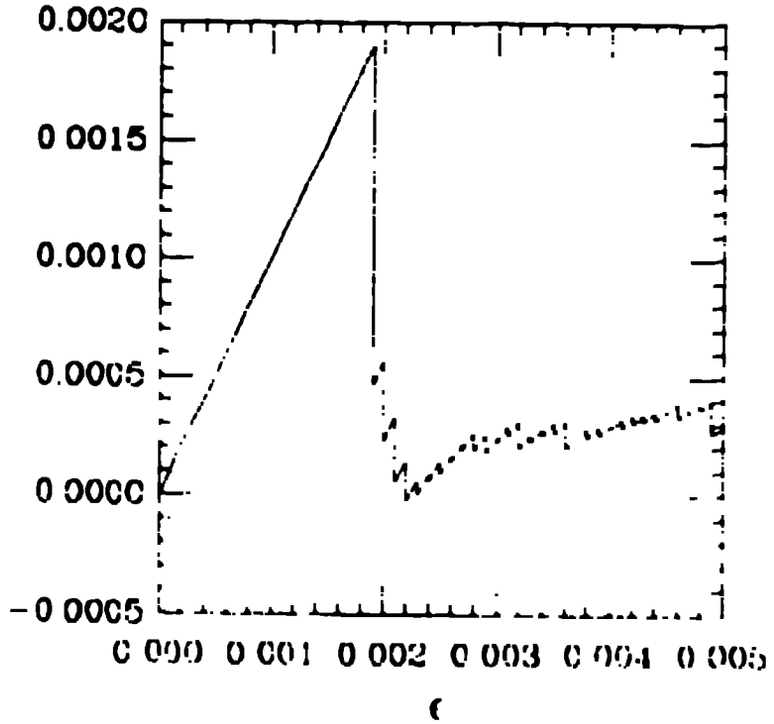
0.0020
0 0015
0.0010
0.0005
0 0000
−0 0005
0 000
0 001
0 002
0 003
0 004
0 005
σ_{xx}
ϵ

(d)

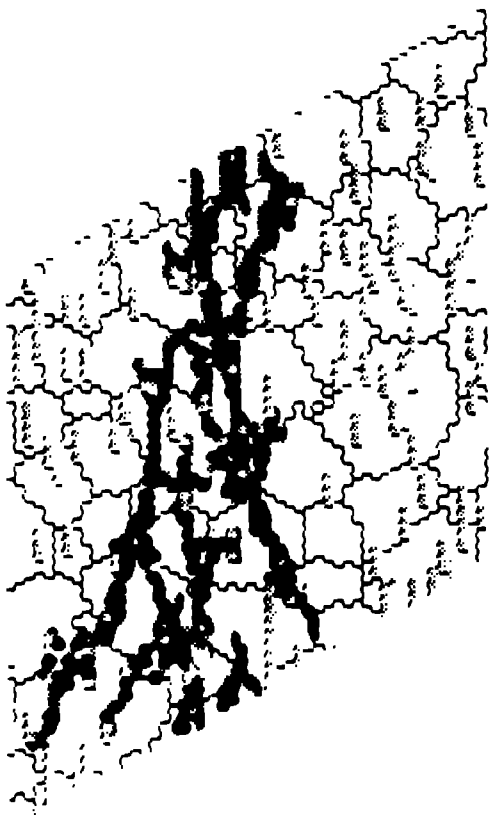

(a)

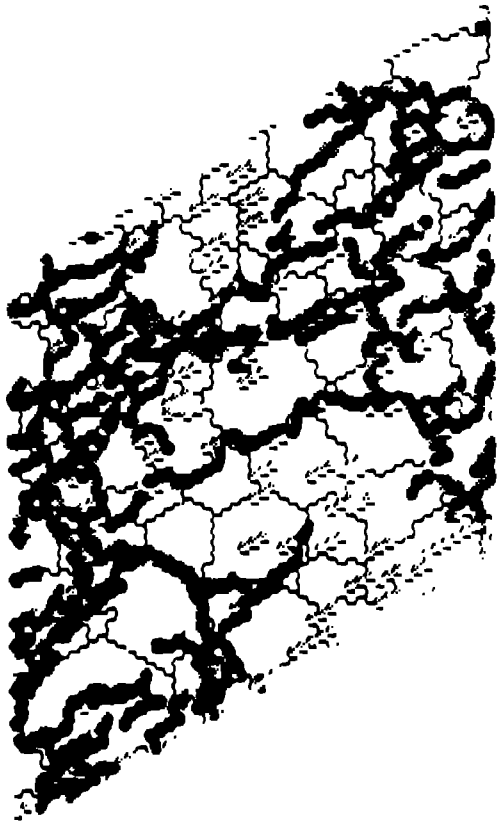

(b)